Tuning electro-optic susceptibity via strain engineering in artificial PZT multilayer films for high-performance broadband modulator

Minmin Zhu [a,b,c], Zehui Du [c], Hongling Li [a], Bensong Chen [c], Lin Jing [a], Roland Ying Jie Tay [c], Jinjun Lin [a], Siu Hon Tsang [c], Edwin Hang Tong Teo [a,b,c,*]

[a] NOVITAS, School of Electrical and Electronic Engineering, Nanyang Technological University, 50 Nanyang Avenue, Singapore 639798

[b] CINTRA CNRS/NTU/THALES, UMI 3288 and Research Techno Plaza, 50 Nanyang Drive, Border X Block, Level 6, Singapore 637553

[c] Temasek Laboratories, Research Techno Plaza, 50 Nanyang Drive, Singapore 637553

E-mail address: htteo@ntu.edu.sg

ABSTRACT

A series of $Pb(Zr_{1-x}Ti_x)O_3$ multilayer films alternatively stacked by $Pb(Zr_{0.52}Ti_{0.48})O_3$ and $Pb(Zr_{0.35}Ti_{0.65})O_3$ layers have been deposited on corning glass by magnetron sputtering. The films demonstrate pure perovskite structure and good crystallinity. A large tetragonality (c/a) of ~ 1.061 and a shift of ~ 0.08 eV for optical bandgap were investigated at layer engineered films. In addition, these samples exhibited a wild tunable electro-optic behavior from tens to ~ 250.2 pm/V, as well as fast switching time of down to a few microseconds. The giant EO coefficient was attribute the strain-polarization coupling effect and also comparable to that of epitaxial (001) single crystal PZT thin films. The combination of high transparency, large EO effect, fast switching time, and huge phase transition temperature in PZT-based thin films show the potential on electro-optics from laser to information telecommunication.

Keywords: PZT; Multilayer; Electro-optic; Strain-polarization; Curie temperature

1. Introduction

Precise manipulation of the light has been a critical component in photonics and optoelectronics from laser to information telecommunications. Electro-optic (EO) materials are allowed to modulate a beam of light, such as the phase, frequency, amplitude, or polarization of the beam without any degrading effects on laser linewidth and stability. Besides, such modulation bandwidth can be extended to the gigahertz range [1,2]. In this case, the linear EO coefficient (r_c) is used to evaluate the modulator performance throughout the phase rotation of the material under the applied electric field [3]. Increasing EO coefficient always brings about more compact and low-cost devices. Currently EO materials such as $LiNbO_3$ (LNO) have been widely applied to amplitude/phase modulator, beam deflector, optical switching, and mode-lock of a laser. However, LNO possesses a relatively low r_c of ~ 30 pm/V which in turn requires high driving voltage or thick materials in LNO-based devices [4]. Among various EO materials, highly textured (001) $Pb(Zr_{1-x}Ti_x)O_3$ (PZT) thin film exhibits high transparency in a UV-visible range (> 80%), low propagation loss (4 dB/cm), large EO coefficient (270.8 pm/V) [5,6], and giant transition temperature (710 ^oC) [7]. Unfortunately, the r_c of polycrystalline PZT thin films (< 100 pm/V) is always far less than that of high textured (001) or epitaxial grown (001) single crystal counterpart reported [5].

Strain engineering has been proven to be an efficient way to improve the ferroelectric properties of perovskite-structured oxide thin films, such dielectric constant [8], piezoelectric constant, and phase transition temperature (T_c) [9,10]. All

the while, design and fabrication of PZT-based heterostructures or artificial multilayer systems to enhance their dielectric and ferroelectric properties have been widely reported. For example, PZT-based multilayer films combining with different perovskite lattice structures such as PZT/$BaTiO_3$ [11], PZT/$PbZrO_3$ [12], PZT/$PbTiO_3$ [13], PZT20/PZT80 [14,15], PZT/(Pb,La)(Zr,Ti)O_3 [16], $(La_{0.7}Sr_{0.3})MnO_3$/PZT [17], and PZT/Pb(Mg, Nb)O_3/PZT [18], have emerged as extremely attractive artificially designed materials, exhibiting a broad range of interface- and strain-mediated phenomena. Notably, the huge tetragonality (*c*/*a)* has been observed in epitaxial PZT/$SrRuO_3$/$SrTiO_3$ heterostructure (*c*/*a* = 1.09) and highly strained polycrystalline PZT multilayer films (*c*/*a* = 1.066) [19,20]. The ferroelectric properties of these films were strongly dependent on the composition and layer structure of the films. It is believed that the strain-polarization coupling is attributed to the enhanced dielectric and ferroelectric properties of these multilayer thin films.[19] However, the optical and electro-optic manipulating in PZT-based multilayer thin films via strain engineering remain unclear. In this letter, we designed PZT-based multilayer films with various layer thicknesses, aiming at studying the interplay relationship between the single layer thickness, the lattice strain, optical and electro-optic properties of the films. The giant r_c of 250.2 pm/V was obtained in highly strained PZT multilayer films, which was 8.3 times larger than that of a commercial LNO-based devices (30 pm/V) and also comparable to those of highly textured (001) or epitaxial (001) PZT thin films.

2. Experimental section

Polycrystalline PZT48 and PZT65 ceramic disk with 10% excess lead were alternately used to deposit PZT-based multilayer films. Corning 1737 glass was firstly coated with a highly (001)-oriented PLT as a seeding layer. Then PZT multilayer films were grown on the PLT-coated corning glass at substrate temperature of ~ 280 ^{o}C and at an O_2/Ar (10:90) gas pressure of ~ 15 mTorr. Five types of multilayer films with almost the same thickness but alternating the one PZT48 and PZT65 layers for a varying period of 5, 8, 10, 15, and 20 have been prepared. Monolayer PZT48 and PZT65 thin films were also deposited under the same conditions for comparison. The films were post-annealed by rapid thermal processor (RTP) under oxygen atmosphere at 650 ^{o}C for 20 mins to obtain good crystallinity. X-ray diffraction (XRD), scanning electron microscopy (SEM), and transmission electron microscopy (TEM) have been used to characterize the engineered PZT multilayer films. Their transmission spectra have been studied by UV-Visible spectrometer at wavelengths between 300 and 900 nm. The EO properties of the films were investigated by modified senarmont method with a He–Ne laser at 632.8 nm. Followed by lithography, e-beam, and lift-off process, coplanar-type gold electrodes (100 nm Au and 10 nm Ti) with a gap of 10 μm were deposited on the films for applying an electric field.

3. Results and Discussion

In these PZT-based multilayer films with a varying stacking period, each period consists of one PZT48 and one PZT65 layer and each layer is with the same thickness. So these films are named as PZT5P, PZT8P, PZT10P, PZT15P, and PZT20P in the following section. Fig. 1a is a schematic illustration of exemplar PZT10P multilayer thin film by

alternatively stacked PZT48 and PZT65 layers. Fig. 1b further demonstrates the cross-section SEM image of the as-grown PZT10P multilayer film on PLT-coated glass substrates. It can be seen that the film thickness is about 1 μm. The interface of each PZT48 and PZT65 layer is clearly differentiated. Energy dispersive spectrometer (EDS) analysis reveals that the as-grown sample only contains three metal elements of Pb, Zr, Ti (not shown). Fig. 1c and 1d show the high-magnitude transmission electron microscopy (HRTEM) image and corresponding selected area diffraction (SAD) pattern of the films, further confirming the excellent crystallinity of PZT-based multilayer film. Noted that the interface is coherent and the *d* spacing of PZT48 and PZT65 layer were 0.290 nm and 0.287 nm, which can be attributed to the (101) planes of PZT, respectively [21]. Notably, the lattice parameter of PZT48 is a little larger than that of PZT65, which is further confirmed by XRD results of monolayer PZT48 and PZT65 under the same condition (not shown). A shift to lower angle at (001) peak of PZT48 is observed compared to PZT65 thin film, indicating the larger lattice parameter of PZT48 thin film derived from the Bragg equation ($n\lambda = 2d\sin\theta$). Coherent interface is a prerequisite condition to engineer the strain induced by small lattice mismatch between PZT48 and PZT65 layer. With such engineered coherent interface, interesting optical and electro-optic behavior can be finely tuned by the artificial multilayer structure.

Fig. 2a shows the typical XRD patterns of PZT-based multilayer thin films. All the films indicate a pure perovskite structure (ABO_3) without any metaphase (pyrochlore, $A_2B_2O_7$) which always seriously degrade the ferroelectric performance [22]. Besides

the pure perovskite phase, the films are also highly (001)-oriented due to the strain effect [23]. PLT is a good seeding layer to promote the formation of perovskite phase due to its matched lattice parameters (a = 3.92 Å, c = 4.06 Å) and thermal expansion coefficient (4.2 x 10^{-6} / ºC of PLT to 4.7 x 10^{-6} / ºC of PZT) [23,24]. Without PLT as the seeding layer, PZT thin film with pyrochlore phase is a predominant issue [22]. In addition, XRD patterns reveal that all the diffraction peaks slightly shift to lower 2θ with the increase of stacking periods. This can be seen more clearly from the magnified (101) peaks of the films as shown in the inset of Fig. 2a, indicating that the lattice parameters of PZT multilayer films are changed. Therefore the strain associated with lattice mismatch among multilayer structures can be engineered by tailoring the layer thickness. The corresponding lattice parameters and cell volume of the PZT multilayer films have been extracted. Fig. 2b shows the tetragonality (c/a) and cell volume of the PZT multilayer films as a function of the layer thickness (d_T). The tetragonality and cell volume of the films follow a monotonically increasing trend as the layer thickness decreases. Large tetragonality (c/a = 1.061) is obtained when the layer thickness reduces to 25 nm. Similar large tetragonality has been observed in epitaxial PZT/$SrRuO_3$/$SrTiO_3$ heterostructure (c/a = 1.09) and highly strained polycrystalline PZT multilayer films (c/a = 1.066) [19,20]. It therefore indicates there is a large lattice distortion (or strain) in the PZT-based multilayer films due to the engineered interfaces.

The successful fabrication of pure perovskite-structured PZT multilayer thin films makes it possible to study their optical and electro-optical properties. Fig. 3a shows

the optical transmission spectra of PZT multilayer films in the wavelength range of 300 to 900 nm. All the films are highly transparent in the visible to near infrared regions, which is favorable for electro-optic modulators in a wide wavelength. The optical bandgap energy (E_g) of thin film is given by [25]:

$$(\alpha h\upsilon)^2 \propto (h\upsilon - E_g) \quad (1)$$

where α is the absorption constant ($T = A\exp(-\alpha d)$), h is the Planck's constant, υ is the frequency, E_g is the optical band gap, and d is the film thickness. The relationship between $(\alpha h\upsilon)^2$ and $h\upsilon$ is plotted in the inset of Fig. 3a. The E_g can be obtained by extrapolating the linear portion to the photon energy axis. As the stacking period increases, the measured E_g of PZT-based multilayer film systems are 3.57, 3.56, 3.54, 3.52, and 3.49 eV, respectively. These results are in the range of values previously reported for PZT which has a bandgap of 3.4 - 4.0 eV [25,26]. The shift of absorption edge towards lower wavelength with the layer thickness reducing reveals a shift of ~ 0.08 eV for direct optical bandgap. Similarly, thickness-dependent optical bandgap has also been observed in Ni-doping PZT thin films [26]. It is believed that some factors are attributed to this change in band gap, such as quantum size effect, change of volume ratio of grain boundaries and defects, as well as strong residual stress.

The refractive index (n) of PZT multilayer films were also derived from the transmission spectra [27]. Derived refractive indices of the films are shown in Fig. 3b. It can be seen from inset of Fig. 3b that $1/(n^2-1)$ decreases linearly with $1/\lambda^2$, indicating the refractive index of the samples follows to the Sellmeiner dispersion relationship [28]:

$$n(\lambda)^2 = 1 + s_0\lambda_0^2/[1-(\lambda_0/\lambda)^2] \quad (2)$$

Our PZT-based multilayer films have a refractive index from 2.23 to 2.36 at 632.8 nm which is comparable to monolayer PZT thin film (n = 2.215 – 2.431) [25,29]. It is lower than Pb(Mg,Nb)O_3-$PbTiO_3$ (PMN-PT, n = 2.599) and very similar to (Pb,La)(Zr,Ti)O_3 (PLZT, n = 2.345) by prism coupler [30,31]. Noted the BO_6 octahedra in an oxygen-octahedral ABO_3 perovskite-structured ferroelectric thin film dominates its corresponding optical property, the lowest energy oscillator is the largest contributor to the dispersion of the refractive index [5]. Another cause for the refractive index variation in PZT-based films should be some void networks imposed by interface, surface roughness, and porosity inside the film.

Using a 632.8 nm He–Ne laser as light source, an ellipsometric amplitude modulator in a modified Senarmont compensator style is used to evaluate the electro-optic performance of PZT-based multilayer films [32]. Fig. 4a and 4b show a schematic and photgraph of the EO modulator based PZT multilayer films. The relationship between the r_c and the birefringence phase shift ($\Delta\Phi$) is given by ($\Delta\Phi = 2\pi l\Delta n/\lambda$), where l is the film thickness, Δn is the birefringence shift, λ is the wavelength. In this setup, the angle between two polarizers is 90^o, which can assure that no modulated signal is observed without any applied electric field. One compensator is inserted to minimize some measuring errors induced by the glass substrate and other optical accessories. Under a certain applied electric field, modulation of the light transmitted the PZT thin film can be received by a detector. Fig. 4c shows the as-deposited PZT-based multilayer films with planar electrode

arrays. In each unit cell, the Au/Ti electrode area is 4 x 4 mm^2, as well as a 10 μm gap along the central axis. As shown in Fig. 4d, the laser goes through the planar electrode pattern with a small gap and then shines on the PZT-based samples with random domains. In fact, (001)-/(101)-oriented PZT thin film possesses normal 90^o domain whereas (111)-oriented one exhibits complex and nano-twinned ferroelectric domain structures with high densities of 90^o domain walls [33]. Our as-grown PZT thin films are polycrystalline and considerably possess random domain structure. The optical image of the Au/Ti electrode pattern further confirms that the gap is 10 μm along the central axis (Fig. 4e).

The relationship between the field-induced birefringence shift (Δn) and the applied electric field (E) at room temperature is given by [34]:

$$\Delta n = -\frac{1}{2} n^3 r_c E \tag{3}$$

Most electro-optic materials belong to a broad of transparent perovskite-structured ferroelectric materials. Fig. 5a exhibits a strong modulation behavior in PZT20P thin film as the applied electric field increasing. The corresponding switching time in PZT20P thin film is about 5.62 μs, as shown in Fig. 5b. Notably, the switching time almost doesn't change with the increasing of E. This fast switching response is comparable to the theoretical and experimental results in transverse EO thin films based on PZT and PMN-PT [35,36]. Such fast and stable switching behavior also demonstrates the potential of PZT-based multilayer films on electro-optics. Fig. 5c shows the change in birefringence (Δn) of PZT-based multilayer films as functions of E. All the samples exhibit a linear EO behavior (Pockels effect) and strong multilayer

structure-dependent EO effects can be observed as well. Fig. 5d, 5e, 5f, 5h, and 5i demonstrate the histograms of the derived EO coefficients in PZT-based multilayer systems. Both PZT48 and PZT65 with 1 μm in thickness are also prepared under the same condition for comparison. Fig. 5j demonstrates the linear EO coefficient (r_c) and switching time (τ) as a function of the layer thickness (d_T). The mean r_c of five PZT multilayer films were determined to be 23.8 ±4.9, 62.9 ±4.6, 105.2 ±4.1, 159.5 ±7.4, and 250.2 ±7.5 pm/V, respectively. Although the polycrystalline characteristic of our PZT multilayer films doesn't examine the individual tensor components of EO effect (r_{33} or r_{31}) due to their randomly oriented domain structure, here the r_c is a compound effect which is always measured and reported to evaluate the EO response in materials [34]. Moreover, the r_c of the films exhibit a wild tailoring range from tens to 250.2 pm/V. The maximum value of 250.2 pm/V obtained is ~34.9 % higher than that of PZT48 monolayer films (181.3 ±9.1 pm/V) and almost 3.0 times higher than that of the PZT65 monolayer film (84.3 ±6.0 pm/V) under the same conditions. In addition, the value of PZT20P thin film is almost 8.3 times higher than the state-of-the-art thin film LNO (commonly r_c = 30 pm/V). It is believed that the giant EO response is more closely with the large strain-induced tetragonality in artificial multilayer structures. Such large strain is also applied to improve the spontaneous polarization and dielectric constant of PZT thin films [19,20]. On the other hand, the corresponding switching time (τ) of these PZT-based materials are calculated to be 4.42, 4.51, 4.68, 4.93, and 5.62 μs, respectively. As the layer thickness reduces, the switching time increases slightly due to the more interface induced. In addition, differences between

(001)/(101) and (111) orientation in PZT thin films maybe broaden switching characteristics, which should also be responsible for the observed variation in the switching time [30]. These giant EO responses and fast switching time have made PZT the material of choice for a variety of electro-optic applications ranging from laser to optical telecommunication.

EO modulator based on transparent perovskite thin films is a well-established device and is an essential part in telecommunication industry. The "half-wave" voltage ($V_\pi=(\lambda d)/(n^3 r_c L)$) of traditional EO modulators using a Mach-Zehnder interferometer architecture is inversely proportional to r_c. Apparently, large r_c means the lower operation voltage and low cost in practice. Fig. 6 shows the comparison of r_c in this work with other PZT thin films previously reported in a literature. Our former study reveals that the EO coefficients of PZT thin film strong depend on the structure phase and the orientation [25]. PZT48 thin film at morphotropic phase boundary (MPB) possesses the largest EO coefficient compared with tetragonal PZT65 and rhombohedral PZT20 thin films. Similar giant EO coefficient in PMN-PT system occurs in the composition that lies at the rhombohedral-to-tetragonal phase boundary [30]. In addition, different from very lower r_c in (101)/(111) or polycrystalline PZT thin films (< 134 pm/V) [37,38,39], highly textured (001) or epitaxial (001) PZT thin films exhibit better EO coefficient (240 - 270 pm/V) [5,6,40]. It is worth noting that our engineered PZT20P thin films demonstrate excellent EO performance (250.2 pm/V) which is comparable to those of epitaxial (001) or highly textured (001) PZT thin films. The observed correlation of the EO effect with the

layer thickness is a consequence of the dominating influence of electrostatic boundary conditions.

Fig. 7a compares the EO performance of PZT-based thin films with other EO materials. Most of the state-of-the-art electro-optic materials are based on lead-free and lead-based transparent perovskite-structured ferroelectrics. The former includes $BaTiO_3$ (BT) [41,42], $(Ba,Sr)TiO_3$ (BST) [43,44], $LiNbO_3$ [4], $(K,Na)NbO_3$ (KNN) [45], and $BiFeO_3$ (BFO) [35,46], while the latter contains $(Pb,La)TiO_3$ (PLT) [47], PLZT [48], PMN-PT [30], and PZT [5], etc. Notably, lead-base PZT thin films demonstrate some unbeatable advantages, especially giant Pockels coefficient. Conversely, most lead-free EO materials (LNO, KNN, and BFO) possess a very small r_c (< 30 pm/V), except BTO and its derivative (BST). However, BTO and its derivatives (BST) always demonstrate a low phase transition temperature (T_c) just above room temperature [46], thereby causing instabilities for modulators operating over wide temperature ranges. Typically, materials demonstrate ferroelectricity only below T_c, and are paraelectric above T_c. So high-T_c transparent ferroelectric thin film is required for broadband EO modulators. Fig. 7b demonstrates the comparison of T_c of PZT-based thin films with other EO materials. Compared with lead-free EO thin films such as BTO and BST with a low T_c (< 130 ^oC), most lead-based EO counterparts always possess high T_c (> 300 ^oC) such as PLZT and PZT, as well as large EO coefficient of > 180 pm/V at the same time. In addition, the T_c of PZT48 and PZT20P multilayer films are 419.3 and 488.2 ^oC (inset of Figure 7b), thereby indicating PZT-based devices possess a wild operation range. This is also a significant

improvement on T_c of up to 710 ^oC in PZT/$SrRuO_3$ thin films by molecular beam epitaxy (MBE) [7]. The $1/\varepsilon$ versus (T-T_c) curves in ZPT48 and PZT20P thin films is also measured. Both exhibit a linear behavior which agrees well with Curie-Weiss relationship in typical ferroelectric thin films ($1/\varepsilon=(T-T_c)/C$). Apparently, combination with high transparency, giant r_c, fast switching response, and high T_c, PZT-based materials demonstrate the potential for fast-switching broadband electro-optics in a wide operation range.

4. Conclusions

In summary, strain-engineered PZT multilayer films consisting of PZT48 and PZT65 layers were deposited on PLT-coated coring glass substrates by magnetron sputtering. The layer engineered films exhibit a pure perovskite structure and good crystallinity, as well as a large tetragonality (c/a = 1.061) and a shift of ~ 0.08 eV for optical bandgap. The PZT-based multilayer films have excellent EO coefficients that should lead to more contact and low-cost modulators. We attribute the huge EO effect to the strain-polarization coupling. Remarkably, PZT thin films demonstrate both a fast switching response and a high phase transition temperature that can make them work quickly in a wide operation range. Our study shed light on the potential of PZT-based thin films on electro-optics and telecommunication.

Acknowledgements

The authors would like to acknowledge the funding support from NTU-A*STAR Silicon Technologies Centre of Excellence under the program grant (No. 1123510003)

and Singapore Ministry of Education Academic Research Fund (Tier 2 No. MOE2013-T2-2-050).

REFERENCES:

[1] S.K. Korotky, G. Eisenstein, R.S. Tucker, J.J. Veselka, G. Raybon. Appl. Phys. Lett. 50 (1987), 1631.

[2] D.G. Girton, S.L. Kwiatkowski, G.F. Lipscomb, R.S. Lytel, Appl. Phys. Lett. 58 (1991), 1730.

[3] B.W. Wessels, Annu. Rev. Mater. Res. 37 (2007), 659.

[4] C.L. Sones, P. Ganguly, Y.J. Ying, F. Johann, E. Soergel, R.W. Eason, S. Mailis, Opt. Express 17 (2009), 23755.

[5] M.M. Zhu, Z.H. Du, J. Lin, Alfred L.Y. Tok, Edwin H.T. Teo, Appl. Phys. Lett. 107 (2015), 031907.

[6] J.P. George, P.E. Smet, J. Botterman, V. Bliznuk, W. Woestenborghs, D.V. Thourhout, K. Neyts, J. Beeckman, ACS Appl. Mater. Interfaces, 7 (2016), 13350.

[7] A. Sambri, S. Gariglio, A.T. Pardo, J.M. Triscone, O. Stéphan, J.W. Reiner, C.H. Ahn, Appl. Phys. Lett. 98 (2011), 012903.

[8] D.G. Schlom, L.Q. Chen, C.B. Eom, K.M. Rabe, S.K. Streiffer, J.M. Triscone, Annu. Rev. Mater. Res. 37 (2007), 589.

[9] K.J. Choi, M. Biegalski, Y.L. Li, A. Sharan, J. Schubert, R. Uecker, P. Reiche, Y.B. Chen, X.Q. Pan, V. Gopalan, L.Q. Chen, D.G. Schlom, C.B. Eom, Science 306 (2004), 1005.

[10] J.H. Haenl, P. Irvin, W. Chang, R. Uecker, P. Reiche, Y.L. Li, S. Choudhury, W. Tian, M.E. Hawley, B. Cralgo, A.K. Tagantsev, X.Q. Pan, S.K. Strelffer, L.Q. Chen, S.W. Klrchoefer, J. Levy, D.G. Schlom, Nature 430 (2004), 758.

[11] M.T. Kesim, J. Zhang, S.P. Alpay, L.W. Martin, Appl. Phys. Lett. 105 (2014), 052901.

[12] J.H. Jang, K.H. Yoon, Appl. Phys. Lett. 75 (1999), 130.

[13] L.L. Sun, O.K. Tan, W.G. Zhu, J. Appl. Phys. 99 (2006), 094108.

[14] C. Wang, Q. F. Fang, Z. G. Zhu, A. Q. Jiang, S. Y. Wang, B. L. Cheng, Z. H. Chen, Appl. Phys. Lett. 82 (2003), 2880.

[15] J. G. Wu, D. Q. Xiao, J. G. Zhu, J. L. Zhu, J. Z. Tan, Q. L. Zhang, Appl. Phys.

Lett. 90 (2007), 082902.

[16] Hyeong-Ho. Park, Hyung-Ho. Park, R.H. Hill, Appl. Surf. Sci. 237 (2000), 427.

[17] Z.H. Tang, M.H. Tang, X.S. Lv, H.Q. Cai, Y.G. Xiao, C.P. Cheng, J. He, J. Appl. Phys. 113 (2013), 164106.

[18] Y.X. Tang, B. Zhu, F.F. Wang, D.Z. Sun, Z.J. Hu, X.M. Qin, W.Z. Shi, Appl. Surf. Sci. 371 (2016), 160.

[19] H.N. Lee, S.M. Nakhmanson, M.F. Chisholm, H.M. Christen, K.M. Rabe, D. Vanderbilt, Phys. Rev. Lett. 98 (2007), 217602.

[20] H. Liu, X.G. Gong, J.E. Liang, X.D. Li, D.Q. Xiao, J.G. Zhu, Z.H. Pu, Appl. Phys. Lett. 91 (2007), 122906.

[21] Y.K. Fu, S.Y. Gong, X.F. Liu, G. Xu, Z.H. Ren, X. Li, G.R. Han, J. Mater. Chem. C, 3 (2015), 382.

[22] Z.H. Du, M.M. Zhu, T.S. Zhang, J. Ma, J. Am. Ceram. Soc. 93 (2010), 4036.

[23] M.M. Zhu, Z.H. Du, J. Ma, J. Appl. Phys. 106 (2009), 023113.

[24] Y.M. Kang, J.K. Ku, S. Baik, J. Appl. Phys. 78 (1995), 2601.

[25] M.M. Zhu, Z.H. Du, J. Ma, J. Appl. Phys. 108 (2010), 113119.

[26] S. Kumari, N. Ortega, D.K. Pradhan, A. Kumar, J. Scott, R.S. Katiya, J. Appl. Phys. 118 (2015), 184103.

[27] J.C. Manifacier, J. Gasiot, J.P. Fillard, J. Phys. E 9 (1976), 1002.

[28] W.C. Liu, C.L. Mak, K.H. Wong, D.Y. Wang, H.L. W. Chan, J. Appl. Phys. 100 (2006), 033507.

[29] C.K. Kao, C.H. Tsai, I.N. Lin, Appl. Phys. Lett. 83 (2003), 3915.

[30] X.M. Wan, H.S. Luo, X.Y. Zhao, D.Y. Wang, H.L.W. Chan, C.L. Choy, Appl. Phys. Lett. 85 (2004), 5233.

[31] Z.H. Du, T.S. Zhang, M.M. Zhu, J. Ma, J. Appl. Phys. 105 (2009), 061612.

[32] M.M. Zhu, J. Wu, Z.H. Du, Roland Y.J. Tay, H.L. Li, B. Özyilmaz, Edwin H.T. Teo, Nanoscale, 7 (2015), 14730.

[33] R.J. Xu, S. Liu, I. Grinberg, J. Karthik, A.R. Damodaran, A.M. Rappe, L.M. Martin, Nat. Mater. 14 (2015), 79.

[34] A.D. Dupuy, Y. Kodera, J.E. Garay, Adv. Mater. 28 (2016), 7970.

[35] M.M. Zhu, Z.H. Du, Q. Liu, B.S. Chen, S.H. Tsang, Edwin H.T. Teo, Appl. Phys. Lett. 108 (2016), 233502.

[36] M.M. Zhu, X.L. Chen, Z.H. Du, J. Ma, AIP Advances, 1 (2011), 042163.

[37] C.E. Land, J. Am. Ceram. Soc. 72 (1989), 2059.

[38] K. Kurihara, M. Kondo, K. Sato, M. Ishii, N. Wakiya, K. Shinozaki, Jpn. J. Appl. Phys. 46 (2007), 6929.

[39] T.D. Kang, B. Xiao, V. Avrutin, Ü. Özgür, H. Morkoc, J.W. Park, H.S. Lee, H. Lee, X.Y. Wang, D.J. Smith, J. Appl. Phys. 104 (2008), 093103.

[40] J.J. Choi, G.T. Park, H.E. Kim, D.Y. Kim, Thin Solid Films, 515 (2006), 2437.

[41] C. Xiong, W.H.P. Pernice, J.H. Ngai, J.W. Reiner, D. Kumah, F.J. Walker, C.H. Ahn, H.X. Tang, Nano Lett. 14 (2014), 1419.

[42] S. Abel, S. Thilo, C. Marchiori, C. Rossel, M.D. Rossell, R. Erni, D. Caimi, M. Sousa, A. Chelnokov, B.J. Offrein, J. Fompeyrine, Nat. Commun. 4 (2013), 1671.

[43] D.Y. Wang, J. Wang, H.L.W. Chan, C.L. Choy, J. Appl. Phys. 101 (2007), 043515.

[44] D.Y. Wang, S. Li, H.L.W. Chan, C.L. Choy, Appl. Phys. Lett. 96 (2010), 061905.

[45] S.I. Khartsev, M.A. Grishin, A.M. Grishin, Appl. Phys. Lett. 86 (2005), 062901.

[46] D. Sando, P. Hermet, J. Allibe, J. Bourderionnet, S. Fusil, C. Carrétéro, E. Jacquet, J.C. Mage, D. Dolfi, A. Barthélémy, Ph. Ghosez, M. Bibes, Phys. Rev. B 89 (2014), 195106.

[47] A. Boudrioua, J.C. Loulergue, E. Dogheche, D. Remiens, J. Appl. Phys. 85 (1999), 1780.

[48] T. Fujii, T. Suzuki, Y. Fujimori, T. Nakamura, M. Moriwake, H. Takasu, Jpn. J. Appl. Phys. 45 (2006), 7520.

FIGURE CAPTURES:

Fig. 1. (a) Schematic configurations of PZT multilayer thin film with periodic compositional PZT65 and PZT48 layers. (b) Cross-section SEM image of PZT10P thin films. (c) HRTEM image of the interface between PZT48 and PZT65 layer, as well as (d) the corresponding SAD pattern.

Fig. 2. (a) XRD patterns of PZT-based multilayer thin films. The inset is the slow scan of the films at (101) peak. (b) Tetragonality (c/a) and cell volume of the samples as a function of layer thickness d_T.

Fig. 3. (a) Transmission spectra of PZT-based multilayer thin films. The inset is the plots of $(\alpha h\upsilon)^2$ versus $(h\upsilon)$ for the films. The optical bandgap energy is obtained by applying a baseline method. (b) Refractive indices of the samples as a function of wavelength. The inset indicates the linear relationship between $1/(n^2\text{-}1)$ and $1/\lambda^2$.

Fig. 4. (a) Schematic of the modified senarmont compensator amplitude modulator. (b) Photograph of our custom-built amplitude modulator based on PZT-based multilayer films. (c) Photograph of the as-grown samples on glass substrates with Au/Ti electrode arrays on their surface. (d) Schematic indicating the laser shines on the polycrystalline PZT-based samples with the planar electrode pattern. (e) Optical image of one planar electrode with a 10 μm gap along the central axis.

Fig. 5. (a) Electric-field-controllable optical modulation in PZT20P thin film under various applied electric field. (b) The corresponding switching time in PZT20P thin film as the applied electric field increases. (c) Change in birefringence (Δn) of PZT-based multilayer films as a function of the applied electric field. The histograms of the linear EO coefficients of (d) PZT20P, (e) PZT15P, (f) PZT10P, (h) PZT8P, and (i) PZT5P thin films. (j) The r_c and τ of the films as functions of layer thickness (d_T).

Fig. 6. Comparing the EO coefficient r_c of PZT-based multilayer films with other PZT thin films previously reported.

Fig. 7. Comparison of (a) electro-optic coefficient (r_c) and (b) phase transition temperature (T_c) of PZT-based multilayer films with other common EO materials. The inset is the temperature-dependent dielectric constants of PZT48 monolayer and PZT20P multilayer films.

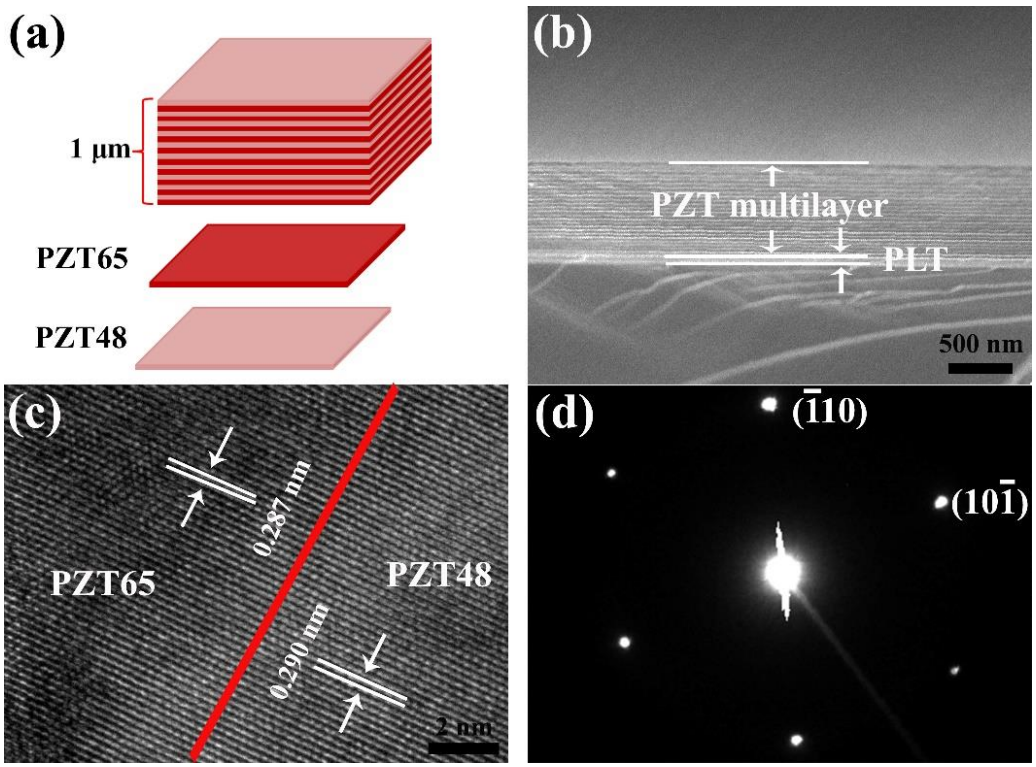

Fig. 1. (a) Schematic configurations of PZT multilayer thin film with periodic compositional PZT65 and PZT48 layers. (b) Cross-section SEM image of PZT10P thin films. (c) HRTEM image of the interface between PZT48 and PZT65 layer, as well as (d) the corresponding SAD pattern.

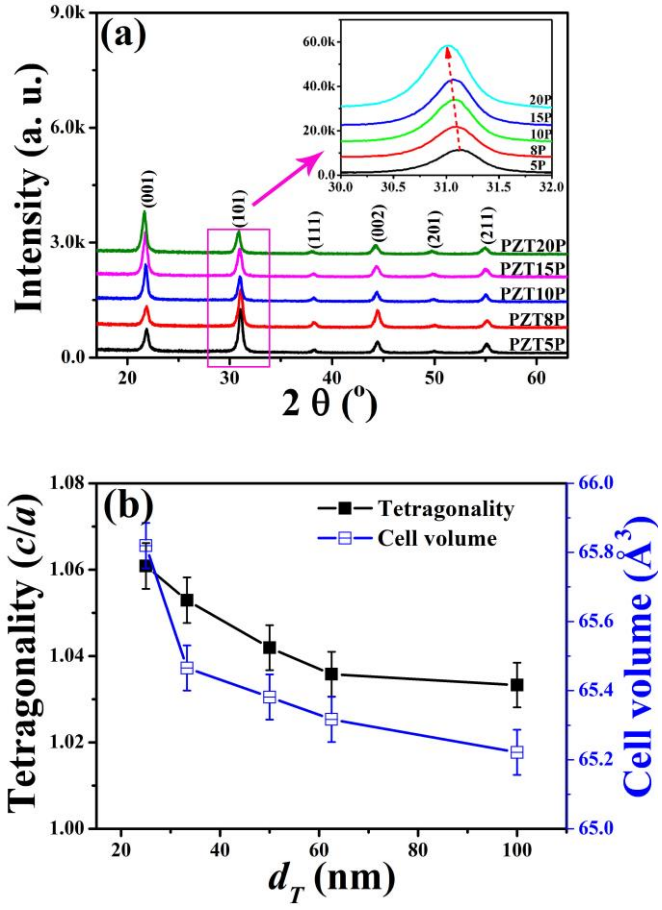

Fig. 2. (a) XRD patterns of PZT-based multilayer thin films. The inset is the slow scan of the films at (101) peak. (b) Tetragonality (*c*/*a*) and cell volume of the samples as a function of layer thickness d_T.

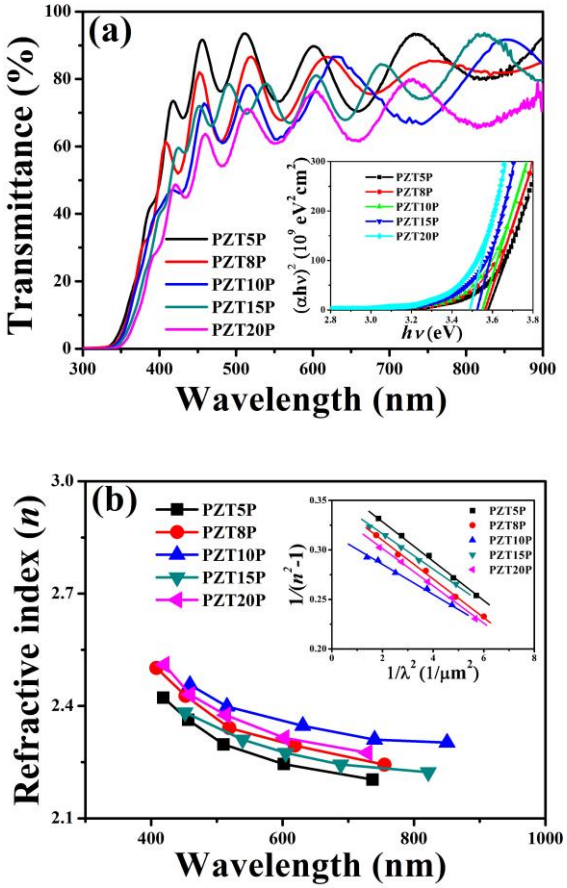

Fig. 3. (a) Transmission spectra of PZT-based multilayer thin films. The inset is the plots of $(\alpha h\upsilon)^2$ versus $(h\upsilon)$ for the films. The optical bandgap energy is obtained by applying a baseline method. (b) Refractive indices of the samples as a function of wavelength. The inset indicates the linear relationship between $1/(n^2\text{-}1)$ and $1/\lambda^2$.

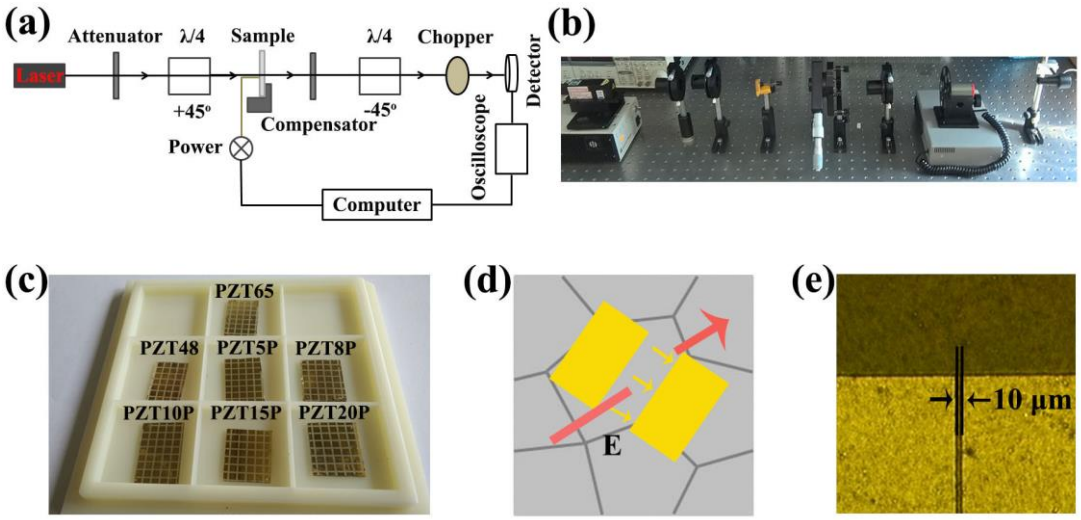

Fig. 4. (a) Schematic of the modified senarmont compensator amplitude modulator. (b) Photograph of our custom-built amplitude modulator based on PZT-based multilayer films. (c) Photograph of the as-grown samples on glass substrates with Au/Ti electrode arrays on their surface. (d) Schematic indicating the laser shines on the polycrystalline PZT-based samples with the planar electrode pattern. (e) Optical image of one planar electrode with a 10 μm gap along the central axis.

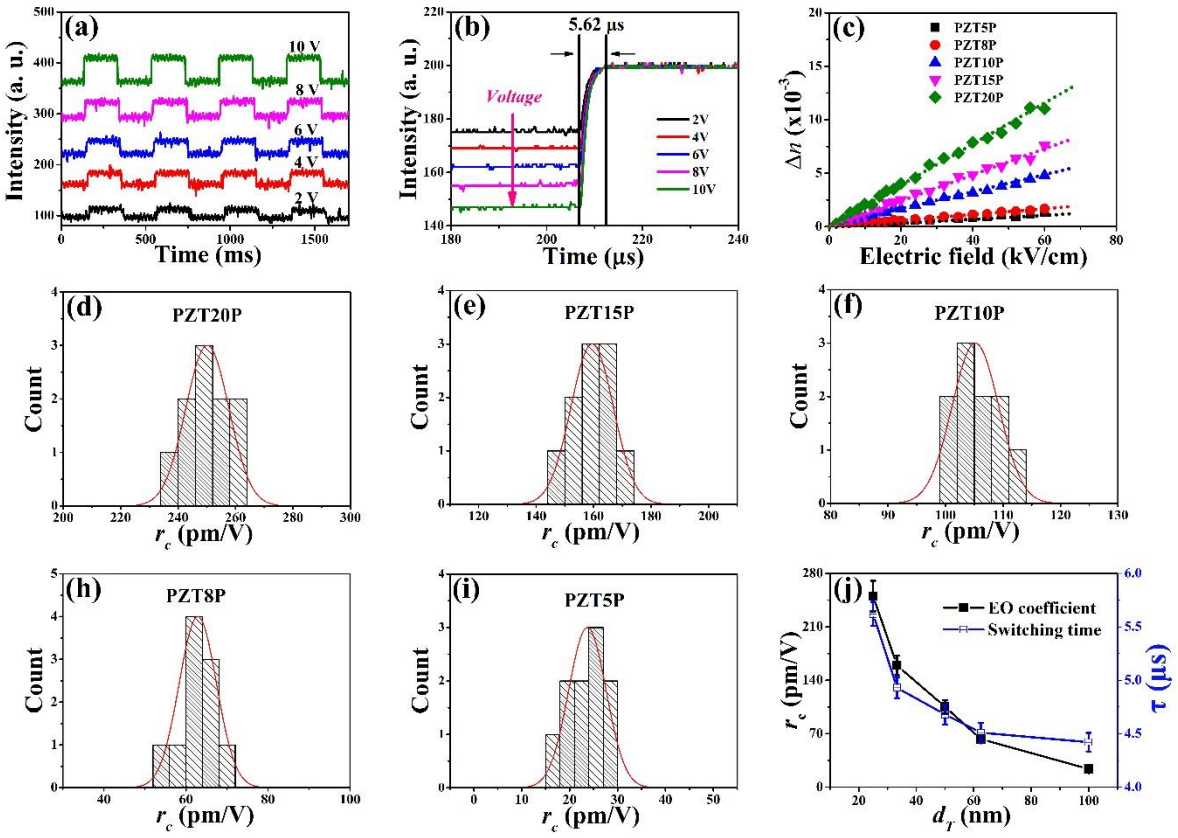

Fig. 5. (a) Electric-field-controllable optical modulation in PZT20P thin film under various applied electric field. (b) The corresponding switching time in PZT20P thin film as the applied electric field increases. (c) Change in birefringence (Δn) of PZT-based multilayer films as a function of the applied electric field. The histograms of the linear EO coefficients of (d) PZT20P, (e) PZT15P, (f) PZT10P, (h) PZT8P, and (i) PZT5P thin films. (j) The r_c and τ of the films as functions of layer thickness (d_T).

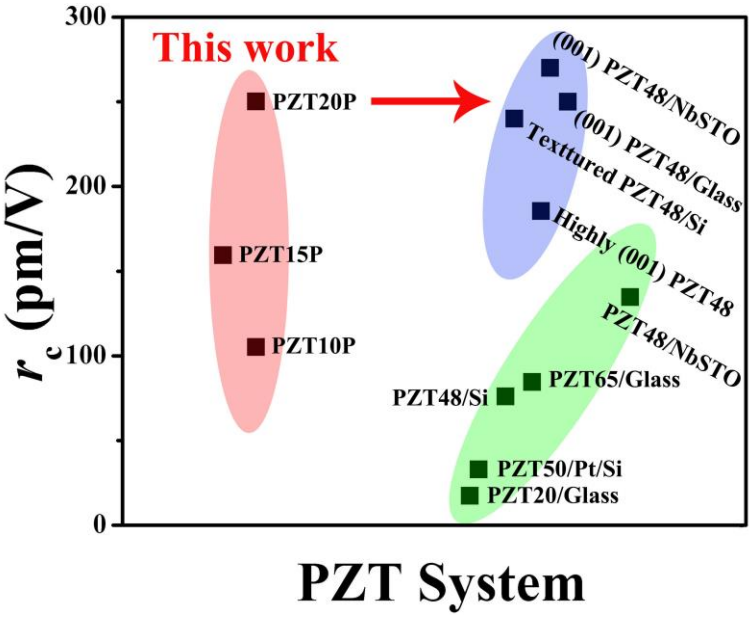

Fig. 6. Comparing the EO coefficient r_c of PZT-based multilayer films with other PZT thin films previously reported.

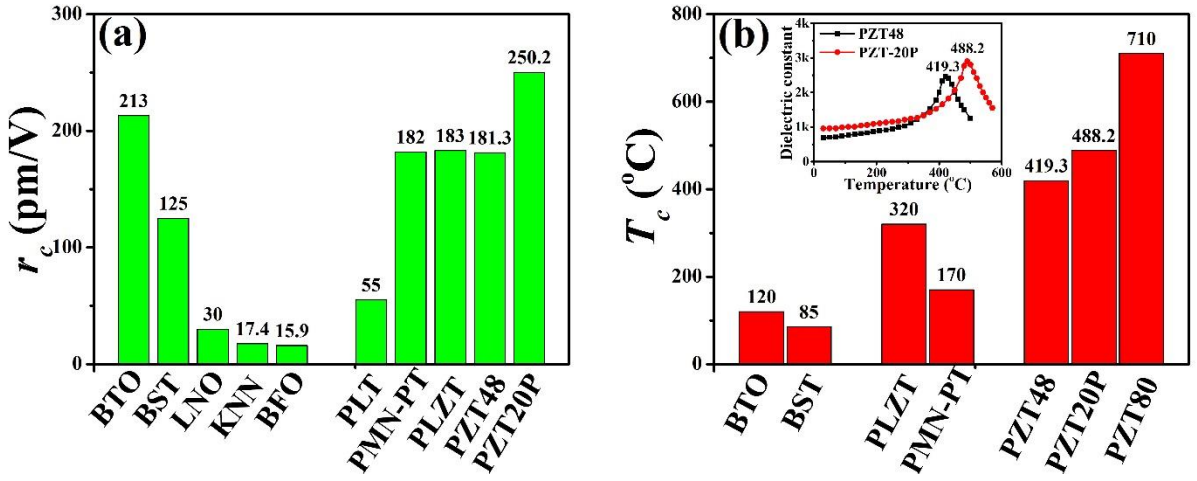

Fig. 7. Comparison of (a) electro-optic coefficient (r_c) and (b) phase transition temperature (T_c) of PZT-based multilayer films with other common EO materials. The inset is the temperature-dependent dielectric constants of PZT48 monolayer and PZT20P multilayer films.